

Collision of drops with inertia effects in strongly sheared linear flow fields

By FRANCK PIGEONNEAU^{1,2†}
AND FRANÇOIS FEUILLEBOIS¹

¹PMMH (Physique Thermique), ESPCI, 10, rue Vauquelin 75231 Paris Cedex 05, France

²ONERA, BP 72, 29, avenue de la division Leclerc 92322 Chatillon Cedex, France

(Received 31 January 2000 and in revised form 26 September 2001)

The relative motion of drops in shear flows is responsible for collisions leading to the creation of larger drops. The collision of liquid drops in a gas is considered here. The drops are small enough for the Reynolds number to be low (negligible fluid motion inertia), yet large enough for the Stokes number to be possibly of order unity (non-negligible inertia in the motion of drops). Possible concurrent effects of Van der Waals attractive forces and drop inertia are taken into account.

General expressions are first presented for the drag forces on two interacting drops of different sizes embedded in a general linear flow field. These expressions are obtained by superposition of solutions for the translation of drops and for steady drops in elementary linear flow fields (simple shear flows, pure straining motions). Earlier solutions adapted to the case of inertialess drops (by Zinchenko, Davis and coworkers) are completed here by the solution for a simple shear flow along the line of centres of the drops. A solution of this problem in bipolar coordinates is provided; it is consistent with another solution obtained as a superposition of other elementary flow fields.

The collision efficiency of drops is calculated neglecting gravity effects, that is for strongly sheared linear flow fields. Results are presented for the cases of a simple linear shear flow and an axisymmetric pure straining motion. As expected, the collision efficiency increases with the Stokes numbers, that is with drop inertia. On the other hand, the collision efficiency in a simple shear flow becomes negligible below some value of the ratio of radii, regardless of drop inertia. The value of this threshold increases with decreasing Van der Waals forces. The concurrence between drop inertia and attractive van der Waals forces results in various anisotropic shapes of the collision cross-section. By comparison, results for the collision efficiency in an axisymmetric pure straining motion are more regular. This flow field induces axisymmetric sections of collision and strong inertial effects resulting in collision efficiencies larger than unity. Effects of van der Waals forces only appear when one of the drops has a very low Stokes number.

1. Introduction

Collisions of liquid drops dispersed in a gas are responsible for the creation of larger drops. The prediction of such events is an important problem for various applications in nuclear and chemical engineering, environmental sciences, etc.

† Present address: Saint-Gobain Recherche, BP 135, 39 quai Lucien Lefranc, F-93303 Aubervilliers Cedex, France.

The formation of a large drop from two smaller ones may be described in two steps:

(i) a close approach of the two drops because of a shear flow or a difference in their velocities of sedimentation; this step is directed by various factors: hydrodynamic forces due to the flows outside and inside the drops, drop inertia and van der Waals attractive forces between their surfaces;

(ii) a deformation of the close surfaces leading to their coalescence. Chesters (1991) established that, in a shear flow, the ratio of the magnitude of the deformation to the drop radius is proportional to the square root of the capillary number. Here, the capillary number is typically of the order of 10^{-6} so that the deformation is about a factor 10^3 smaller than the drop radii.

This article is only concerned with the first step. That is, calculations of approaching drops will be stopped at small gaps before deformation occurs. For these small gaps, we will say that 'collision' occurs, although we do not calculate the subsequent phenomena leading to contact and drops coalescence.

Drops considered here are small enough for the Reynolds numbers of the flows outside and inside the drops to be low and Stokes equations to apply. Nevertheless, inertia may be important in the motion of drops since the ratio of the density of the liquid to that of the gas is large. The consistency of these various assumptions will be made clear in § 2.

The influence of drop inertia when in sedimentation was taken into account by Hocking & Jonas (1970) and Jonas (1972). They used expressions for the forces on particles derived by Stimson & Jeffery (1917). Jonas (1972) also used a correction factor in order to account for the effect of gas rarefaction between two close drops, at the last stage of collision. Davis (1984) calculated the collision efficiency of sedimenting solid spheres. He determined their relative trajectories, using the coefficients for the forces on the spheres derived by Jeffrey & Onishi (1984). He also introduced the effects of gas rarefaction and van der Waals forces.

The collision of drops in linear flow fields was studied by Wang, Zinchenko & Davis (1994). Their calculation only applies to small drops in aerosols, or to hydrosols, since they do not consider drop inertia.

The goal of this article is a systematic study of the influence of drop inertia on the collision of drops in linear flow fields. The article structure is the following.

Section 2 is devoted to a discussion of the various assumptions. Sedimentation effects are neglected in the calculation of collisions. Here, the shear rate is assumed to be strong enough for the shear flow velocity to be larger than the fluid velocity due to sedimentation. Van der Waals forces are taken into account but gas rarefaction effects are not considered in the collision step. The assumptions are discussed by calculating orders of magnitude of the various non-dimensional numbers. Ranges of parameters compatible with the assumptions are displayed for the typical case of water drops in air.

A comprehensive set of results for the hydrodynamic forces on two drops in a general linear flow field is presented in § 3. The formulation uses a superposition of elementary linear flow fields. Earlier results for such flow fields are complemented here by the solution for two drops at rest in a shear flow aligned with their line of centres. This problem is solved by the technique of bipolar spherical coordinates. A verification is also provided by superposition of other elementary flow fields. Finally, a tensorial expression is provided for the general expressions for the forces.

These results for the forces are used in § 4 to calculate the collision efficiency of drops in linear shear flows, namely a simple shear flow and an axisymmetric pure straining

motion. Although the same results allow the more general problem of sedimentation in a general linear flow field to be considered, the calculations would require a more complicated treatment of three-dimensional trajectories which is outside the scope of this article. Equations of motion of the drops with the expressions for the forces from §3 are integrated to provide their trajectories. The collision efficiency is determined from relative trajectories for which collisions occur.

Results are presented and discussed in §5. Finally, the conclusion is in §6.

2. Discussion of assumptions and orders of magnitude

Consider two drops with radii a_1 and a_2 , with $a_2 \leq a_1$. The dispersed phase (the drops) is denoted with a subscript d and the continuous phase with a subscript c . Let ρ be the density, μ and ν the dynamic and kinematic viscosities, respectively. Relevant non-dimensional numbers are the ratio of radii $\lambda = a_2/a_1$, the density ratio $\hat{\rho} = \rho_d/\rho_c$ and the viscosity ratio $\hat{\mu} = \mu_d/\mu_c$. Let γ denote a characteristic shear rate of the flow field.

Inertia in the motion of fluids is neglected. That is, we assume that the drops are small enough for the Reynolds numbers of the flows outside and inside the drops to be small. In the continuous phase, it is sufficient to write the condition for the flow around the largest drop:

$$Re_c = \frac{\gamma a_1^2}{\nu_c} \ll 1. \quad (2.1)$$

It is assumed that the drop interface is clean, namely that there is no interfacial film. Then the condition of continuity of tangential stresses at the interface gives $v_c = \hat{\mu} v_d$, where v denotes a characteristic value of the fluid velocity in each phase. With $v_c = \gamma a_1$, the Reynolds number for the flow inside drop 1 is

$$Re_d = \frac{v_d a_1}{\nu_d} = \frac{\hat{\rho}}{\hat{\mu}^2} Re_c. \quad (2.2)$$

This number is assumed to be small, and so is that for the flow inside drop 2.

The inertia in the motion of drop 1 is characterized by the Stokes number St_1 , which is introduced in a natural way in the dimensionless equation of motion (4.1a). The reference quantities used there and throughout the article are γ^{-1} for the time, $(a_1 + a_2)/2$ for the lengths, $v_\gamma = \gamma(a_1 + a_2)/2$ for the velocities and $3\pi\mu_c\gamma(a_1 + a_2)^2/2$ for the forces. Using (2.1), the Stokes number is written as

$$St_1 = \frac{4}{9} Re_c \frac{\hat{\rho}}{1 + \lambda}. \quad (2.3)$$

Drop inertia is important when St_1 is of order unity or larger. From (2.1)–(2.3), it is seen that:

- (a) $St_1 = O(1)$ and $Re_d \ll 1$ require that $\hat{\mu} \gg 1$,
- (b) $St_1 = O(1)$ and $Re_c \ll 1$ require that $\hat{\rho} \gg 1$,

which is the case of drops of liquid in a gas (typically, water drops in air).

In the calculations of the relative trajectories of two drops (§4), sedimentation forces will be assumed to be negligible compared with the shear forces. The relevant sedimentation velocity for encounters between drops is the relative velocity, which is of the order of the difference of the velocities of drops falling in isolation; from

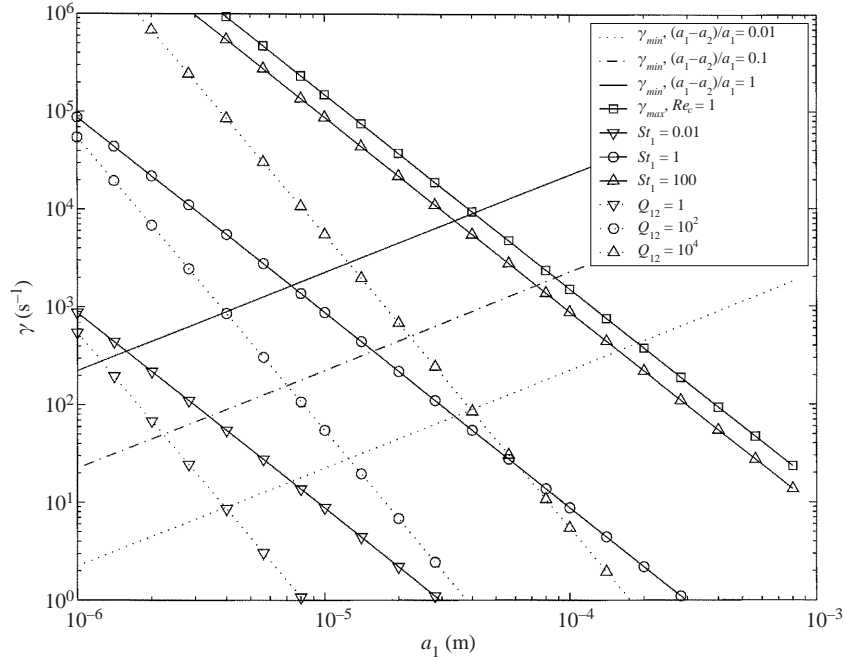


FIGURE 1. Map of shear rate γ versus the radius of the largest drop a_1 for water drops in air.

Hadamard (1911) and Rybczynski (1911)

$$\Delta v_d = \frac{2}{9} \frac{a_1^2 - a_2^2}{v_c} \frac{\hat{\mu} + 1}{\hat{\mu} + 2/3} (\hat{\rho} - 1)g, \quad (2.4)$$

where g is the acceleration due to gravity. The assumption states that Δv_d is negligible compared with the characteristic velocity v_γ for the shear flow. This condition provides a lower value γ_{min} for γ .

It will now be shown how the shear rate γ can be large enough for this condition to apply, while keeping the above assumption of small Reynolds numbers and still allowing the Stokes number to be of order unity. All these conditions are represented in a map of γ versus a_1 , figure 1, for the typical case of water drops in air. The lower bound γ_{min} is represented for various values of the relative difference in radii, $(a_1 - a_2)/a_1$. The condition $Re_c \ll 1$ appears as an upper bound γ_{max} for γ . Lines of constant Stokes number St_1 (with $\lambda = 1$) are displayed. Admissible ranges of the drop size and monodispersity and of the shear rate combine to give a set of values for which the present model applies.

Typical applications of the present model are flows of dispersions of drops with a shear rate of 10^3 to 10^5 s^{-1} , such as in nozzles, strongly sheared layers, jets and boundary layers.

For environmental applications, it is questionable whether the model applies to the formation of large drops in cumulus clouds. It is recognized that drops forming by condensation tend to become of uniform size (Jonas 1996): since $d(a^2)/dt \simeq \text{constant}$, da/dt is larger for small drops and smaller for large drops. Because of this monodispersity, we expect relative sedimentation effects to be small compared with shear flow effects. In cumulus clouds with a strong convection, the rate of dissipation of turbulent energy, ϵ , is approximately 0.15 W kg^{-1} (Fuchs 1964). For air,

the Kolmogorov scale $\eta_K = (v_c^3/\epsilon)^{1/4}$ then is around $400\ \mu\text{m}$. For drops smaller than η_K , the flow may be locally considered as a shear flow, with a rate of shear $\gamma = \sqrt{\epsilon/v_c} \approx 100\ \text{s}^{-1}$. Consider for instance drops with radii $a_1 = 10\ \mu\text{m}$ and $a_2 = 9.9\ \mu\text{m}$. From figure 1, their relative velocity of sedimentation is about $1/5$ of the shear flow velocity, and neglecting it would be a rough approximation. Moreover, the Stokes number is small (around 0.1) so that the present analysis is not useful for this case. A Stokes number of order unity would correspond to a shear rate that would be about 10 times larger, that is $\gamma \sim 10^3\ \text{s}^{-1}$. Thus, a description of drops collisions in cumulus clouds would require the study of the combined effects of relative sedimentation and shear flows. We leave this point for further research.

The relative importance of attractive van der Waals forces may also be questioned. These forces are expressed as the gradient of a potential, Φ_{12} . Omitting the retardation effect, the classical expression obtained by Hamaker (1937) is for unequal particles:

$$\Phi_{12}(s) = -\frac{A}{6} \left\{ \frac{8\lambda}{(s^2 - 4)(1 + \lambda)^2} + \frac{8\lambda}{s^2(1 + \lambda)^2 - 4(1 - \lambda)^2} + \ln \left[\frac{(s^2 - 4)(1 + \lambda)^2}{s^2(1 + \lambda)^2 - 4(1 - \lambda)^2} \right] \right\}, \quad (2.5)$$

where A is the Hamaker constant (that is of the order of 10^{-19} J) and $s = 2r/(a_1 + a_2)$, where r is the distance between the sphere centres. A dimensionless number comparing hydrodynamic and van der Waals forces is

$$Q_{12} = \frac{(a_1 + a_2)v_\gamma}{2(m_1 + m_2)A} \quad (2.6)$$

where m_α is the mobility of drop α . From the expression for the drag force on a drop derived by Hadamard (1911) and Rybczynski (1911):

$$m_\alpha = \frac{1}{6\pi\mu_c a_\alpha} \frac{\hat{\mu} + 1}{\hat{\mu} + 2/3}. \quad (2.7)$$

Lines for $Q_{12} = 1, 10^2, 10^4$ are plotted for the case $\lambda = 1$ in figure 1. In general, van der Waals forces are efficient for small drops and inertia for large drops. However, the figure shows that for small drops it is possible that $Q_{12} = 10^3$ (giving a significant effect on the collision efficiency, as will be presented later) while $St_1 = 1$. Another representation of the relative effects of drop inertia and van der Waals forces is the product of non-dimensional numbers $St_1 Q_{12} = (a/l)^5$, where the length l varies like $\gamma^{-2/5}$. A typical value of l for equal water drops in air is $1\ \mu\text{m}$ for $\gamma = 10^4\ \text{s}^{-1}$. From this discussion, it appears that the calculation of collisions should include van der Waals forces together with drop inertia.

Another possible physical effect on small drops is Brownian motion. The relative effect of Brownian motion is represented by the Péclet number:

$$Pe_{12} = \frac{(a_1 + a_2)v_\gamma}{D_{12}}, \quad (2.8)$$

where D_{12} is a constant of the order of the relative diffusion coefficient of the pair of drops. It may be taken as $D_{12} = kT(m_1 + m_2)$, where k is Boltzmann's constant and T the absolute temperature. As drops considered here are larger than a micron, $Pe_{12} \gg 1$ so that Brownian motion is negligible.

Finally, our assumption that gas rarefaction effects are negligible requires a lower bound for the sizes of the gaps that we consider, since the mean free path in air

is of the order of $0.05\ \mu\text{m}$. For smaller gaps, there would also be drop deformation together with rarefaction effects. We leave these effects for further research.

3. Hydrodynamic forces on two drops in a general linear flow field

Expressions for the hydrodynamic forces acting on two solid spherical particles embedded in a general flow field are now well known. A collection of results is provided, e.g. in the handbook of Kim & Karrila (1991). By comparison, results for two drops are not so comprehensive.

Drops considered here are spherical, and the classical boundary conditions of continuity of fluid velocity and tangential stress apply on their surfaces. From the linearity of Stokes equation, expressions for the forces acting on two drops moving with given velocities in a general linear flow field can be written as the sum of forces on the drops moving with these velocities in a fluid at rest and forces on the drops at rest in the linear flow field.

The first problem is well documented. Its solutions will be recalled briefly here since it is also needed for the second problem. Again by linearity of the Stokes equations, the drag forces \mathbf{F}_1 , \mathbf{F}_2 on the drops in a fluid at rest depend on their velocities \mathbf{V}_1 , \mathbf{V}_2 through linear relationships:

$$\mathbf{F}_1 = -6\pi\mu_c a_1 (\mathbf{A}_{11} \cdot \mathbf{V}_1 + \mathbf{A}_{12} \cdot \mathbf{V}_2), \quad (3.1a)$$

$$\mathbf{F}_2 = -6\pi\mu_c a_2 (\mathbf{A}_{21} \cdot \mathbf{V}_1 + \mathbf{A}_{22} \cdot \mathbf{V}_2). \quad (3.1b)$$

The $\mathbf{A}_{\alpha\beta}$ (where $\alpha, \beta = 1, 2$) are second-rank tensors with components (using the notation of Jeffrey 1992):

$$A_{ij}^{(\alpha\beta)} = X_{\alpha\beta}^A d_i d_j + (\delta_{ij} - d_i d_j) Y_{\alpha\beta}^A, \quad (3.2)$$

where \mathbf{d} is the unit vector along the line of centres. The $X_{\alpha\beta}^A$ and the $Y_{\alpha\beta}^A$ are non-dimensional frictions coefficients depending on the ratio $\hat{\mu}$ of viscosities, on the ratio λ of radii and on the dimensionless distance s between the centres of the drops. The $X_{\alpha\beta}^A$ correspond to a motion of the drops 1, 2 along their line of centres and the $Y_{\alpha\beta}^A$ to a motion perpendicular to that line.

Unlike the general expressions for solid spherical particles, equations (3.1) do not contain rotation velocities of the drops. This is because the torque on a drop vanishes in any flow field (see Appendix A). Thus, the rotation velocities of the drops are linearly dependent on their translational velocities and are incorporated systematically in (3.1). That is, these equations are analogous to those for freely rotating solid particles.

Expressions for these frictions coefficients as series in $1/s$ were obtained by Hetsroni & Haber (1978). These relations are valid for large s and were obtained from the method of reflections. Results for the forces on close drops ($\xi = s - 2 \ll 1$) moving along their line of centres were computed by Davis, Schonberg & Rallison (1989) using a boundary collocation technique. Their result for $X_{\alpha\beta}^A$ is provided in term of Padé approximants:

$$X_{11}^A = \lambda X_{22}^A = \frac{2\lambda^2}{(1+\lambda)^3 \xi} f(m), \quad X_{12}^A = \lambda X_{21}^A = -X_{11}^A, \quad (3.3a, b)$$

with

$$f(m) = \frac{1 + 0.38m}{1 + 1.69m + 0.43m^2}, \quad m = \frac{1}{\hat{\mu}} \sqrt{\frac{2\lambda}{(1+\lambda)^2 \xi}}, \quad \text{and } \xi = s - 2. \quad (3.4a, b)$$

	$\lambda = 0.5$	$\lambda = 1$
$\xi = 10^{-4}$	0.5407	0.5264
$\xi = 10^{-3}$	0.7853	0.7753
$\xi = 10^{-2}$	0.9199	0.9155

TABLE 1. Values of $f(m)$ defined in (3.4) for $\hat{\mu} = 100$.

The possibility of collision is reduced by the large values of the friction coefficients for small gaps: e.g. $X_{11}^A \sim 10^3$ for the closest separations ($\xi = 10^{-4}$) considered in our calculation of the collisions of drops. The function $f(m)$ in (3.4) represents the ratio of the friction coefficients for drops to those for solid particles. Values of this function for drops in air ($\hat{\mu} = 100$) are displayed in table 1. It can be as low as 0.5 for $\xi = 10^{-4}$. Thus, when calculating collisions, it is necessary to take into account the flows inside drops, despite the apparently large ratio of viscosities between the drops and the surrounding gas.

There are no lubrication results similar to (3.3) and (3.4) for the $Y_{\alpha\beta}^A$, that is for the forces on close drops moving perpendicular to their line of centres. The only available estimate is provided by Zinchenko (1982):

$$Y_{\alpha\beta}^A(\xi, \lambda, \hat{\mu}) = Y_{\alpha\beta}^A(0, \lambda, \hat{\mu}) + O(|\ln \xi|^{-1}). \quad (3.5)$$

Results for the friction coefficients on drops at intermediate distances were calculated with the method of bispherical polar coordinates (Jeffery 1912): the $X_{\alpha\beta}^A$ were obtained by Haber, Hetsroni & Solan (1973) and the $Y_{\alpha\beta}^A$ by Zinchenko (1980). This completes the presentation of the solutions for two drops moving in a fluid at rest.

Results for two drops at rest embedded in a general linear flow field are not comprehensive at present and this problem will now be studied in detail. The unperturbed velocity in a general linear flow field is written as

$$\mathbf{U}^\infty(\mathbf{x}) = \mathbf{U}_0^\infty + \boldsymbol{\Omega}^\infty \times \mathbf{x} + \mathbf{E}^\infty \cdot \mathbf{x}, \quad (3.6)$$

where the velocity \mathbf{U}_0^∞ , the vorticity $\boldsymbol{\Omega}^\infty$ and the rate-of-strain tensor \mathbf{E}^∞ are constants. Denoting the constant unperturbed velocity gradient $\boldsymbol{\Gamma} = \nabla \mathbf{U}^\infty$, the rate-of-strain tensor is written explicitly as its symmetric expression: $\mathbf{E}^\infty = (\boldsymbol{\Gamma} + {}^t\boldsymbol{\Gamma})/2$.

Results for the forces were obtained with the method of bispherical polar coordinates. The position \mathbf{x}_{O_b} of the origin O_b of these coordinates (cf. figure 2) is calculated from the positions of the sphere centres \mathbf{x}_1 and \mathbf{x}_2 by

$$\mathbf{x}_{O_b} = \left[\frac{1}{2} + \frac{2(\lambda - 1)}{s^2(1 + \lambda)} \right] \mathbf{x}_1 + \left[\frac{1}{2} - \frac{2(\lambda - 1)}{s^2(1 + \lambda)} \right] \mathbf{x}_2. \quad (3.7)$$

Changing the frame of reference, the flow field is decomposed into two parts:

$$\mathbf{U}^\infty(\mathbf{x}) = \underbrace{\mathbf{U}_0^\infty + \boldsymbol{\Omega}^\infty \times \mathbf{x}_{O_b} + \mathbf{E}^\infty \cdot \mathbf{x}_{O_b}}_{\mathbf{U}^{(I)\infty}} + \underbrace{\boldsymbol{\Omega}^\infty \times (\mathbf{x} - \mathbf{x}_{O_b}) + \mathbf{E}^\infty \cdot (\mathbf{x} - \mathbf{x}_{O_b})}_{\mathbf{U}^{(II)\infty}(\mathbf{x} - \mathbf{x}_{O_b})}, \quad (3.8)$$

namely a constant flow field and a linear flow field in the framework with origin \mathbf{x}_{O_b} .

Forces for the constant flow field are obtained by noting that the problem is equivalent to that of two drops moving with the same velocity $-\mathbf{U}^{(I)\infty}$ in a fluid at rest. It is thus sufficient to replace \mathbf{V}_1 and \mathbf{V}_2 by $-\mathbf{U}^{(I)\infty}$ in equations (3.1).

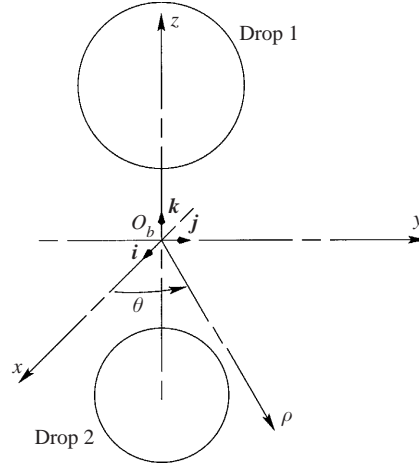


FIGURE 2. Reference frame of the bispherical polar coordinates.

Defining $\mathbf{x}_b = \mathbf{x} - \mathbf{x}_{O_b}$, the second part of the unperturbed flow field is rewritten as

$$\mathbf{U}^{(II)\infty}(\mathbf{x}_b) = \mathbf{\Gamma} \cdot \mathbf{x}_b. \quad (3.9)$$

From linearity of the Stokes equations, the forces on the drops are obtained by superposition of expressions obtained for simpler flow fields, namely simple shear flows and pure straining motions. Some of these flow fields give zero force, as can be found using symmetry arguments and the reversibility of Stokes equations, in the spirit of Bretherton (1962). Details of the decomposition may be found in Pigeonneau (1998). With these results, the drag forces can be written in term of a limited number of coefficients:

$$\mathbf{F}_1^{(II)} = -6\pi\mu_c a_1^2 [(D_1^{xz}\gamma_{xz} + D_1^{zx}\gamma_{zx})\mathbf{i} + (D_1^{yz}\gamma_{yz} + D_1^{zy}\gamma_{zy})\mathbf{j} + D_1^{zz}\gamma_{zz}\mathbf{k}], \quad (3.10a)$$

$$\mathbf{F}_2^{(II)} = -6\pi\mu_c a_2^2 [(D_2^{xz}\gamma_{xz} + D_2^{zx}\gamma_{zx})\mathbf{i} + (D_2^{yz}\gamma_{yz} + D_2^{zy}\gamma_{zy})\mathbf{j} + D_2^{zz}\gamma_{zz}\mathbf{k}], \quad (3.10b)$$

where the γ with subscripts are the components of tensor $\mathbf{\Gamma}$ and \mathbf{i} , \mathbf{j} , \mathbf{k} are the unit vectors, in the $(O_b; x; y; z)$ reference frame depicted in figure 2. The D are friction coefficients. By symmetry, the problems for the shear rates γ_{xz} , γ_{zx} are identical to the ones for γ_{yz} , γ_{zy} , respectively, so that $D_\alpha^{xz} = D_\alpha^{yz}$ and $D_\alpha^{zx} = D_\alpha^{zy}$, for $\alpha = 1, 2$. The D depend on s , λ and $\hat{\mu}$. They are calculated by resolving the three problems represented in figure 3, namely (i) a pure shear flow perpendicular to the line of centres, (ii) one parallel to that line, (iii) a pure straining motion.

In their treatment of neutrally buoyant drops without inertia, Wang *et al.* (1994) used an expression for the mobilities derived by Batchelor & Green (1972). The unperturbed flow field was decomposed as a solid body rotation and a pure straining motion. When inertialess particles are embedded in a solid body rotation flow, they move with the velocity of that flow. Then Wang *et al.* (1994) showed that they only needed to solve the first and third problems in figure 3. Their solution follows the earlier solution of Zinchenko (1980) for the shear flow in the case of equal drops.

On the other hand, here drops with inertia embedded in a solid body rotation flow field do not necessarily follow this flow. For this reason, the second problem in figure 3 has to be resolved. Its solution is obtained here by the method of bispherical polar coordinates, a generalization of the technique of Zinchenko (1980). Details of the derivation of this new solution are given in Appendix B, where results are provided

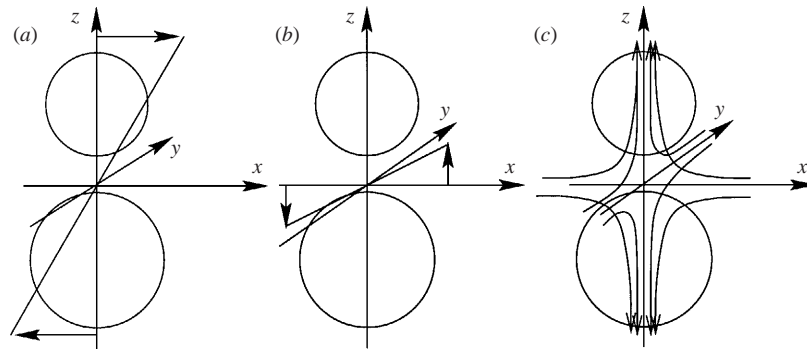


FIGURE 3. The three cases to compute the D friction coefficients; a pure shear flow, (a) perpendicular and (b) parallel to the line of centres; (c) a pure straining motion.

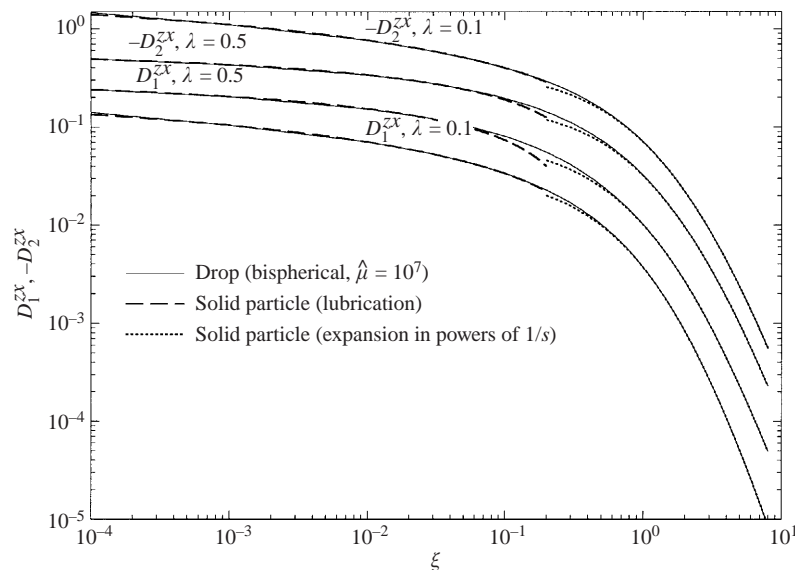


FIGURE 4. The D_1^{zx} and $-D_2^{zx}$ friction coefficients for drops for $\lambda = 0.1, 0.5$ and comparison with solid particles.

for the friction coefficients D_1^{zx} , D_2^{zx} . When the interior viscosity of the drops becomes infinite, for $\hat{\mu} \rightarrow \infty$, the forces on the drops should become equal to those acting on freely rotating solid particles. The friction coefficients D_1^{zx} , D_2^{zx} for solid particles were calculated as expansions for small gaps (lubrication) and for large gaps (expansions in powers of $1/s$) using the results of Kim & Karrila (1991) and Jeffrey (1992) (for details see Pigeonneau 1998). They are compared in figure 4 with those of drops with $\hat{\mu} = 10^7$, for the two different values $\lambda = 0.1$ and 0.5 . The agreement is very good for most of the range.

Alternatively, the coefficients D_1^{zx} and D_2^{zx} for drops can be obtained by another method, thus providing a verification of the calculation in bispherical polar coordinates. It is well known that, from the linearity of the Stokes equations, a shear flow along the line of centres is equivalent to the sum of a shear flow perpendicular to the line of centres and a solid body rotation, as shown in figure 5.

The forces on drops at rest in a fluid moving in solid body rotation are calculated

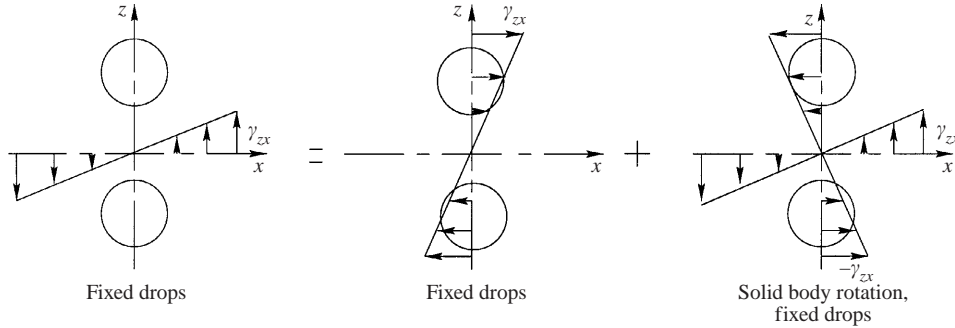


FIGURE 5. Decomposition of the shear flow along the line of centers.

in a framework rotating with the fluid. Since fluid inertia vanishes, they are equal to the drag forces on drops moving with the appropriate velocities in a fluid at rest:

$$F_1^{pr} = -6\pi\mu_c a_1^2 (Y_{11}l_1 - Y_{12}l_2)\gamma_{zx}, \quad (3.11a)$$

$$F_2^{pr} = -6\pi\mu_c a_2 a_1 (Y_{21}l_1 - Y_{22}l_2)\gamma_{zx}, \quad (3.11b)$$

where $a_1 l_\alpha$ is the distance between the origin of the bispherical polar coordinates and the centre of drop α ; in terms of λ and s the non-dimensional distances are

$$l_1 = \frac{s(1+\lambda)}{4} + \frac{1-\lambda}{s}, \quad l_2 = \frac{s(1+\lambda)}{4} - \frac{1-\lambda}{s}. \quad (3.12a, b)$$

The decomposition of figure 5 gives

$$D_\alpha^{zx} = D_\alpha^{xz} + Y_{\alpha 1}^A l_1 - Y_{\alpha 2}^A l_2 \quad (\alpha = 1, 2). \quad (3.13)$$

The friction coefficients $Y_{\alpha\beta}^A$ and D_α^{xz} were calculated with the method of bispherical polar coordinates using the results of Zinchenko (1980) and Wang *et al.* (1994). The resulting values of D_α^{zx} obtained from (3.13) were then found to be identical, within the precision of the numerical calculation, to our result calculated directly by the method of bispherical polar coordinates, equations (B 30a), (B 30b). This agreement provides a verification of the different approaches.

The expansions (3.13) also give more insight when combined with the other elementary flow fields. For after extracting the unperturbed velocity at the centres of the drops, the hydrodynamic forces (3.10) can be written in tensor notation (for details, see Pigeonneau 1998):

$$\mathbf{F}_1^{(II)} = -6\pi\mu_c a_1 [-\mathbf{A}_{11} \cdot \mathbf{U}^{(II)\infty}(\mathbf{x}_{b1}) - \mathbf{A}_{12} \cdot \mathbf{U}^{(II)\infty}(\mathbf{x}_{b2}) + a_1 \mathbf{G}_1 : \mathbf{E}^\infty], \quad (3.14a)$$

$$\mathbf{F}_2^{(II)} = -6\pi\mu_c a_2 [-\mathbf{A}_{21} \cdot \mathbf{U}^{(II)\infty}(\mathbf{x}_{b1}) - \mathbf{A}_{22} \cdot \mathbf{U}^{(II)\infty}(\mathbf{x}_{b2}) + a_1 \mathbf{G}_2 : \mathbf{E}^\infty], \quad (3.14b)$$

where \mathbf{G}_α is a third-rank tensor which must be symmetrical in the last two indices. By similarity with the notation for the forces on solid particles, the general form of \mathbf{G}_α is

$$\mathbf{G}_{ijk}^{(\alpha)} = X_\alpha^G d_i d_j d_k + Y_\alpha^G (d_j \delta_{ik} + d_k \delta_{ij} - 2d_i d_j d_k). \quad (3.15)$$

By identification, we find

$$X_\alpha^G = X_{\alpha 1}^A l_1 - X_{\alpha 2}^A l_2 + D_\alpha^{zz}, \quad (3.16a)$$

$$Y_\alpha^G = Y_{\alpha 1}^A l_1 - Y_{\alpha 2}^A l_2 + D_\alpha^{zx}. \quad (3.16b)$$

Note that from equations (3.13), the coefficients Y_α^G are identical to the D_α^{zx} .

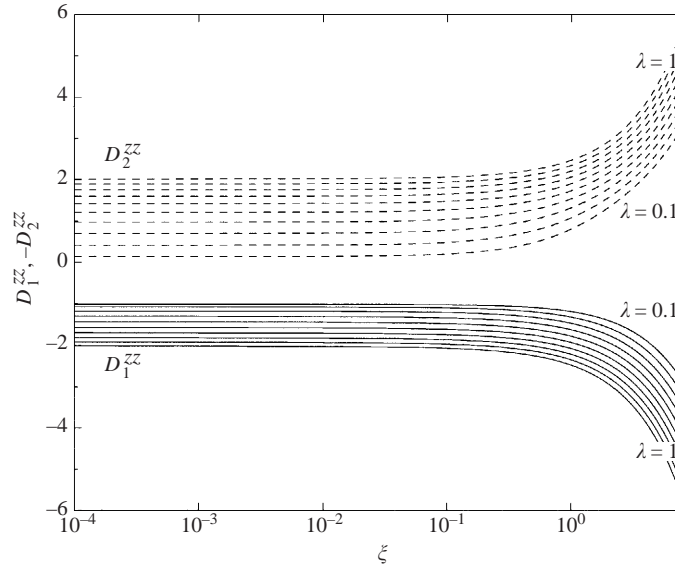


FIGURE 6. Results for D_1^{zz} and D_2^{zz} as functions of the normalized gap ξ for $\hat{\mu} = 100$ and for values of λ from 0.1 to 1 in steps of 0.1. D_1^{zz} is decreasing with λ whereas D_2^{zz} is increasing.

Lubrication expressions for coefficients X_α^G can be obtained by noting that the coefficients D_α^{zz} do not diverge for $\xi \rightarrow 0$. Values of D_α^{zz} calculated in bispherical polar coordinates are plotted in figure 6 for the case of water drops in air, with viscosity ratio $\hat{\mu} \simeq 100$ and for various values of the radii ratio. As a result, first-order approximations for small ξ are sufficient:

$$D_\alpha^{zz}(\xi, \lambda, \hat{\mu}) = D_\alpha^{zz}(0, \lambda, \hat{\mu}) + O(|\ln \xi|^{-1}). \quad (3.17)$$

Using the lubrication expansions (3.3) for the $X_{\alpha\beta}^A$ and (3.12) for the l_α , lubrication expressions for the X_α^G follow:

$$X_1^G(\xi, \lambda, \hat{\mu}) = X_{11}^A(\xi, \lambda, \hat{\mu}) \frac{(\xi + 2)(1 + \lambda)}{2} + D_1^{zz}(0, \lambda, \hat{\mu}), \quad (3.18a)$$

$$X_2^G(\xi, \lambda, \hat{\mu}) = -X_{22}^A(\xi, \lambda, \hat{\mu}) \frac{(\xi + 2)(1 + \lambda)}{2} + D_2^{zz}(0, \lambda, \hat{\mu}). \quad (3.18b)$$

The exact results for X_1^G together with the lubrication expression (3.18a) are represented in figure 7 for $\lambda = 0.1, 0.5$ and 1. Analogous results were obtained for X_2^G and are not represented here.

Taking also into account the first part of the unperturbed flow fields, (3.8), and the motions of the drops, we obtain the final tensorial expressions for the drag forces on drops moving in a general linear flow field:

$$\mathbf{F}_1 = -6\pi\mu_c a_1 \{ \mathbf{A}_{11} \cdot [\mathbf{V}_1 - \mathbf{U}^\infty(\mathbf{x}_1)] + \mathbf{A}_{12} \cdot [\mathbf{V}_2 - \mathbf{U}^\infty(\mathbf{x}_2)] + a_1 \mathbf{G}_1 : \mathbf{E}^\infty \}, \quad (3.19a)$$

$$\mathbf{F}_2 = -6\pi\mu_c a_2 \{ \mathbf{A}_{21} \cdot [\mathbf{V}_1 - \mathbf{U}^\infty(\mathbf{x}_1)] + \mathbf{A}_{22} \cdot [\mathbf{V}_2 - \mathbf{U}^\infty(\mathbf{x}_2)] + a_1 \mathbf{G}_2 : \mathbf{E}^\infty \}. \quad (3.19b)$$

These expressions will now be used to determine the trajectories of two interacting drops, the rate of collision and the collision efficiency.

Note that if the forces were given in the bispherical polar coordinates system, it would be necessary to introduce a rotation matrix between this framework and the

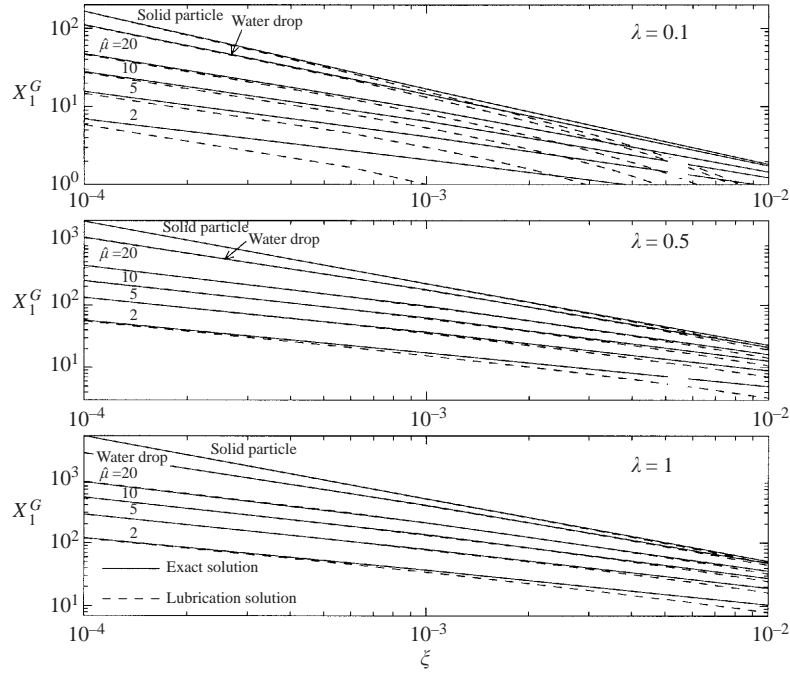


FIGURE 7. X_1^G as a function of ξ for $\lambda = 0.1, 0.5, 1$ and various values of the viscosity ratio $\hat{\mu}$.

absolute frame of reference, as was done by Lin (1968) using Eulerian angles. With the tensorial expressions (3.19a) and (3.19b), the numerical coding is made simpler.

4. Determination of the collision efficiency

4.1. Dimensionless equations of motion

The dimensionless position of drop α will now be denoted \bar{x}_α . The dimensionless momentum and kinematic equations of the drop motion are

$$St_1 \frac{d\mathbf{v}_1(\tau)}{d\tau} = \mathbf{f}_1, \quad \frac{d\bar{x}_1(\tau)}{d\tau} = \mathbf{v}_1, \quad (4.1a, b)$$

$$St_2 \frac{d\mathbf{v}_2(\tau)}{d\tau} = \mathbf{f}_2, \quad \frac{d\bar{x}_2(\tau)}{d\tau} = \mathbf{v}_2, \quad (4.1c, d)$$

where two Stokes numbers appear, St_1 already defined in (2.3) and

$$St_2 = \lambda^3 St_1. \quad (4.2)$$

The dimensionless forces \mathbf{f}^α are sums of hydrodynamic forces and other physical forces. The hydrodynamic dimensionless drag forces are from (3.19a), (3.19b)

$$\mathbf{f}_1^h = -\frac{2}{1+\lambda} \left\{ \mathbf{A}_{11} \cdot [\mathbf{v}_1 - \mathbf{u}^\infty(\bar{x}_1)] + \mathbf{A}_{12} \cdot [\mathbf{v}_2 - \mathbf{u}^\infty(\bar{x}_2)] + \frac{2}{1+\lambda} \mathbf{G}_1 : \mathbf{e}^\infty \right\}, \quad (4.3a)$$

$$\mathbf{f}_2^h = -\frac{2\lambda}{1+\lambda} \left\{ \mathbf{A}_{21} \cdot [\mathbf{v}_1 - \mathbf{u}^\infty(\bar{x}_1)] + \mathbf{A}_{22} \cdot [\mathbf{v}_2 - \mathbf{u}^\infty(\bar{x}_2)] + \frac{2}{1+\lambda} \mathbf{G}_2 : \mathbf{e}^\infty \right\}. \quad (4.3b)$$

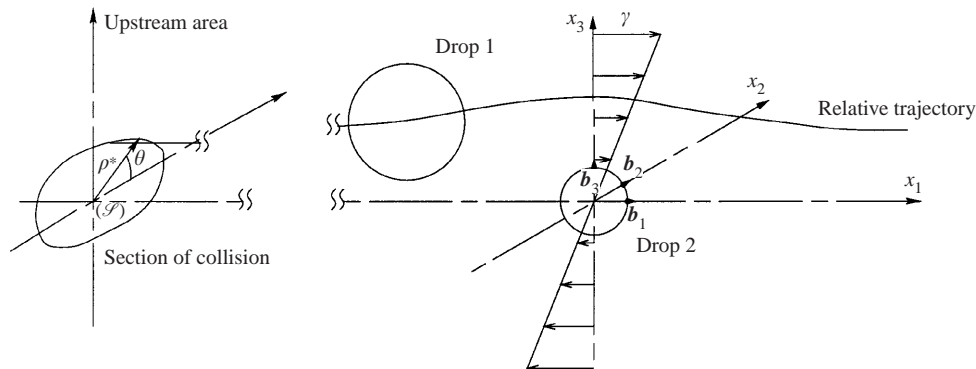


FIGURE 8. Representation of the relative trajectory of the drops and the section of collision.

\mathbf{e}^∞ is the dimensionless rate-of-strain tensor. The other physical forces considered here are attractive van der Waals forces between the drop surfaces. They are written in dimensionless form as

$$\mathbf{f}_1^{vdw} = -\frac{1}{Q_{12}} \frac{2(3\hat{\mu} + 2)\lambda}{3(\hat{\mu} + 1)(1 + \lambda)^2} \frac{d\phi_{12}(s)}{ds} \left(\frac{\mathbf{s}}{s}\right) = -\mathbf{f}_2^{vdw}, \quad (4.4)$$

where $\mathbf{s} = \bar{\mathbf{x}}_1 - \bar{\mathbf{x}}_2$, $s = |\mathbf{s}|$, $\phi_{12} = \Phi_{12}/A$ and Φ_{12} was defined in (2.5).

4.2. Method of calculation of trajectories

Collisions between drops are determined by calculating their relative trajectories. Since drop inertia is taken into account, time appears explicitly in the equations of motion of two interacting drops, (4.1a)–(4.1d). These equations should then be integrated numerically.

When the drops come close together, forces become large and the system of differential equations becomes stiff. An appropriate integration technique is then necessary. A fourth-order method semi-implicit with adapted time step developed by Kaps & Rentrop (1979) was used in the computation.

The solution allows the relative position of the drops to be determined and then the rate of collision and the collision efficiency in a homogeneous cloud of drops to be derived. This approach was used by Hocking & Jonas (1970), Jonas (1972) and Davis (1984) to calculate the collision efficiency of settling spheres.

Two examples of linear flow fields will be treated here: a simple shear flow, §4.3, and an axisymmetric pure straining motion, §4.4.

4.3. Collision efficiency of drops in a simple shear flow

Consider a system of coordinates (x_1, x_2, x_3) , with origin at the centre of drop 2. The unperturbed flow field is the simple shear flow:

$$\mathbf{u}^\infty(\mathbf{x}) = \gamma x_3 \mathbf{b}_1, \quad (4.5)$$

where \mathbf{b}_1 is the unit vector along the x_1 -axis (see figure 8).

The initial position of drop 1 'far' upstream of drop 2 is taken at $s = s^*$. Hydrodynamic interactions and van der Waals forces are neglected at this distance. That is, the velocity of sphere 1 is taken to be that of the surrounding fluid. A polar coordinates system (ρ^*, θ) defined from $x_2 = \rho^* \cos \theta$ and $x_3 = \rho^* \sin \theta$ is used in the upstream area. Values of ρ^* for which the drops collide are sought by a trial and error method. The section in which collisions can occur is obtained by repeating this procedure for

various values of θ . It is sufficient to restrict the calculation to the first quadrant by symmetry.

Once this section of collision is known, the rate of collision in a homogeneous dispersion of drops can be obtained by the classical method of Smoluchowski (1917); the expression for the rate of collision is obtained by integrating the flux over the section of collision \mathcal{S} in the upstream area and multiplying by n_1 and n_2 , the numbers of drops 1 and 2 per unit volume:

$$J_{12} = n_1 n_2 \int_{\mathcal{S}} |\mathbf{V}_{12} \cdot \mathbf{b}_1| dS. \quad (4.6)$$

\mathbf{V}_{12} is the relative velocity between the drops; using its value $\mathbf{V}_{12} = \gamma x_3 \mathbf{b}_1$ in the upstream area, the rate of collision becomes

$$J_{12} = \frac{4}{3} (a_1 + a_2)^3 n_1 n_2 \gamma E_{12}, \quad (4.7)$$

where E_{12} is the collision efficiency defined as

$$E_{12} = \frac{\int_{\mathcal{S}} |x_3| dS}{\frac{4}{3} (a_1 + a_2)^3}. \quad (4.8)$$

Alternatively, using dimensionless coordinates $\bar{x}_i = 2x_i/(a_1 + a_2)$ and a dimensionless section of collision $\bar{\mathcal{S}}$,

$$E_{12} = \frac{3}{32} \int_{\bar{\mathcal{S}}} |\bar{x}_3| d\bar{\mathcal{S}}. \quad (4.9)$$

A value $s^* = 15$ was found to be sufficiently large to describe the upstream area with a good precision. The section of collision was obtained by calculating a few points on its boundary which were then interpolated by cubic splines. The integral for E_{12} was thereafter calculated by the Gauss–Legendre technique.

4.4. Collision efficiency of drops in an axisymmetric pure straining motion

Consider again a system of coordinates (x_1, x_2, x_3) , with origin at the centre of drop 2. The unperturbed flow field is the pure straining motion:

$$\mathbf{u}^\infty(\mathbf{x}) = \gamma(-x_1 \mathbf{b}_1 - x_2 \mathbf{b}_2 + 2x_3 \mathbf{b}_3), \quad (4.10)$$

where \mathbf{b}_i is the unit vector along the x_i -axis. A system of spherical coordinates (R, θ, ϕ) will also be used ($\theta = 0$ denoting the positive x_3 -axis).

The determination of the collision efficiency in this case is simpler: since the flow field is axisymmetric, the section of collision also is axisymmetric; it is determined by only one limit trajectory for which the drops collide in a meridian plane $\phi = \text{constant}$. This trajectory is represented as a solid line in figure 9. It is tangent to the sphere S_c with equation $R = a_1 + a_2$. Its ‘far’ upstream point where hydrodynamic interaction and van der Waals forces are neglected is at $R = R^*$, $\theta = \theta_d$. The dashed line in the figure is the fluid trajectory that is tangent to the sphere S_c at the same point as the drop trajectory. That trajectory starts from $R = R^*$, $\theta = \theta_f$ in the upstream area. By definition, the collision efficiency is the ratio of the incoming flux for the solid line to that for the dashed line. The dotted line in figure 9 is the trajectory that a fluid particle would follow starting from the same upstream point as the drop centre. From the upstream condition that the drop and fluid have equal velocity, the fluxes for the solid line and the dotted line are equal. The collision efficiency thus can also be interpreted as the ratio of the incoming fluid flux for the dotted line to that for

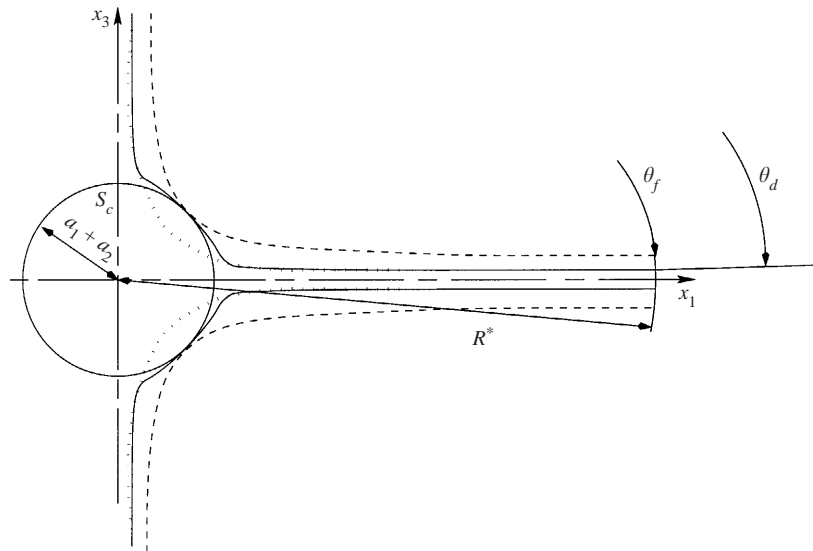


FIGURE 9. Representation of the limit relative trajectory of the drops (solid line) and limit streamline in an axisymmetric pure straining motion.

the dashed line. The expression for the rate of collision was given by Zeichner & Schowalter (1977):

$$J_{12} = \frac{8\pi}{3\sqrt{3}}(a_1 + a_2)^3 \gamma n_1 n_2 E_{12}, \quad (4.11)$$

where the expression for the collision efficiency in term of the dimensionless distance $s^* = 2R^*/(a_1 + a_2)$ is

$$E_{12} = \frac{3\sqrt{3}}{16} s^{*3} \cos \theta_d \sin^2 \theta_d. \quad (4.12)$$

θ_d was calculated as in §4.3 (also with $s^* = 15$).

Note that the case represented in figure 9 is that of an incoming drop with a low inertia; the relative particle trajectory deviates more than the fluid streamlines because of hydrodynamic interactions and the resulting collision efficiency is lower than unity. However, for increasing drop inertia, namely for increasing Stokes number, the drop relative trajectories (solid line) deviate less and less (in the limit of infinite Stokes number, they become parallel). When they deviate less than the streamlines, the collision efficiency is larger than unity.

5. Results and discussion

5.1. Simple shear flow

Consider first the case of drops with a small Stokes number, $St_1 = 10^{-3}$. Values of the collision efficiency E_{12} calculated for various values of the viscosity ratio are presented in figure 10. They are compared with those obtained for inertialess drops ($St_1 = 0$) by Wang *et al.* (1994). There is a threshold of values of λ above which E_{12} becomes non-zero and our values of this threshold are in good agreement with theirs. The collision efficiency decreases with increasing viscosity ratio, and for $\hat{\mu} = 0.1$ and 2 our results also are in good agreement with theirs.

However, a small discrepancy appears for larger values of $\hat{\mu}$, our method giving a

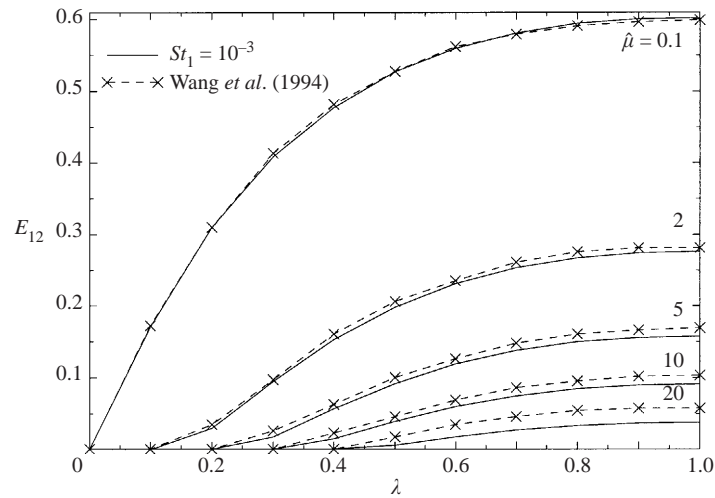


FIGURE 10. Collision efficiency as a function of λ for small Stokes number and various values of the viscosity ratio in simple shear flow. Van der Waals forces are not included.

smaller collision efficiency than Wang *et al.* (1994). Since this disagreement is more important for $\hat{\mu} \sim 10$, it is probably related to the increase of the lubrication forces with a decreasing mobility of the interface. Lubrication forces were accounted for by Wang *et al.* (1994) with two types of solutions: (3.4) for large $\hat{\mu}$ and another one (see their appendix) for a medium range of values of $\hat{\mu}$. Considering the purpose of our application to water drops in air, we only used (3.4) for large $\hat{\mu}$.

We also checked that our result is not affected by possible numerical errors, for when the drops are close together and the Stokes number is small, the system of differential equations is very stiff. We therefore tried another numerical method, the extrapolation semi-implicit method given by Press *et al.* (1992). Results obtained with this alternative method were found to be identical with those computed with the first method, namely with the fourth-order semi-implicit method with adapted time step from Kaps & Rentrop (1979).

The influence of van der Waals forces on collisions was studied in the case of water drops in air, for which the viscosity ratio is approximately 100. It is clear from figure 1 that collisions of drops with a small St_1 and a large Q_{12} cannot be treated without taking gravity effects into account. The physically relevant range for small St_1 is thus limited here to $Q_{12} \leq 10$. Results for E_{12} in terms of Q_{12} are given in figure 11 for the values 0.2, 0.5 and 1 of the radii ratio. There is a good agreement with the results of Wang *et al.* (1994). It may also be remarked that in this range of values of Q_{12} the efficiency varies like $E_{12} \sim Q_{12}^{-1/n}$. The values of n obtained by linear regression in the log-log plot are $n = 2.23, 3.33, 3.71$ for $\lambda = 0.2, 0.5, 1.0$, respectively. For $\lambda = 1$, $n \simeq 4$ is close to the numerical result obtained by Chesters (1991) for collisions of solid particles by van der Waals forces.

After these preliminary verifications for low Stokes number, we now present the main results of this article, which concern the influence of inertia on the collision efficiency. We consider here liquid drops in a gas, e.g. water drops in air, for which the viscosity ratio is approximately 100.

The influence of the Stokes number is displayed in figure 12 which gives E_{12} as a function of λ for various values of St_1 and for $Q_{12} = 10^3$ and 10^4 . As expected, the

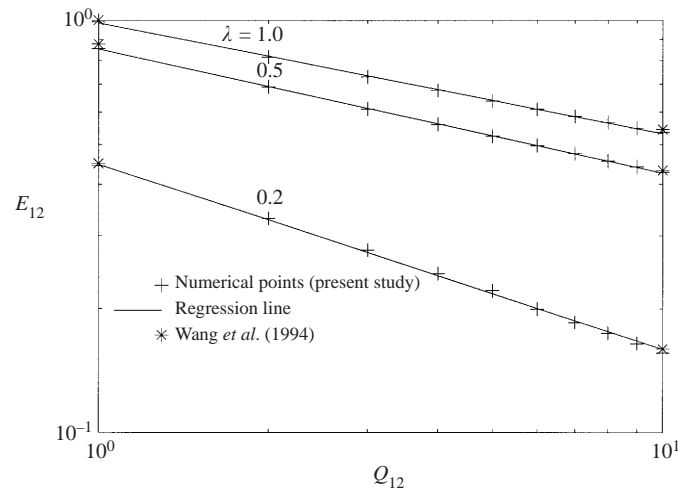


FIGURE 11. Collision efficiency of water drops in air as a function of Q_{12} for small Stokes number, $St_1 = 10^{-3}$, and for $\lambda = 0.2, 0.5,$ and 1 in simple shear flow.

inertia of the drops increases the collision efficiency. For a constant λ , E_{12} increases with St_1 . Since from (4.2) St_2 is proportional to St_1 , E_{12} also increases with St_2 for a constant λ . From (4.2), St_2 is proportional to λ^3 so that E_{12} also increases with St_2 for a constant St_1 . For $Q_{12} = 10^3$, a significant value of E_{12} below $\lambda = 0.2$ could only be obtained with a very large value of St_1 . Thus, there is in practice a threshold at $\lambda = 0.2$, below which E_{12} vanishes. The surprising result is that this threshold appears to be the same for all values of St_1 . For $Q_{12} = 10^4$, the threshold is at $\lambda = 0.3$. Thus, when van der Waals interaction forces are an order of magnitude smaller, there is a dramatic decrease in the collision efficiency of drops in the range of radii such that $0.2 < \lambda < 0.3$. As expected, values of the collision efficiency for $Q_{12} = 10^4$ are smaller than those for 10^3 , since van der Waals attractive forces are weaker. The cross-over of the curves in figure 12 is difficult to interpret physically and should be considered as a numerical artefact, the distance between curves for $0.2 \leq \lambda \leq 0.3$ then giving an estimate of the calculation error on E_{12} .

The collision efficiency was computed for a large range of values of the Stokes number St_1 . It is represented in figure 13 for $Q_{12} = 10^3$ and 10^4 . For a very large Stokes number, E_{12} would reach unity as expected. For the smallest values of the Stokes number, the effect of van der Waals forces becomes more important; there is a small change in curvature in the curves.

The effect of van der Waals forces on the shape of the section of collision is obvious. As an example, figure 14 represents the sections of collision for drops of the same size and various values of the Stokes number. A change in the shape of the section of collision is observed for values of St_1 above $St_1 \simeq 6$. When $St_1 < 6$, the sections of collision are nearly elliptic. When $St_1 \geq 6$, a protuberance appears. The effect of drop inertia can be interpreted as follows. When the line of centres of the drops is close to the plane $\bar{x}_2 = 0$, the difference in the drop velocities is larger than when it is nearly perpendicular to that plane. Inertia effects are thus more important in the first configuration and van der Waals forces in the second configuration. It may thus be understood why the section of collision increases with St_1 close to the plane $\bar{x}_2 = 0$ and does not increase close to the plane $\bar{x}_3 = 0$. Analogous sections of collision were obtained for $Q_{12} = 10^4$.

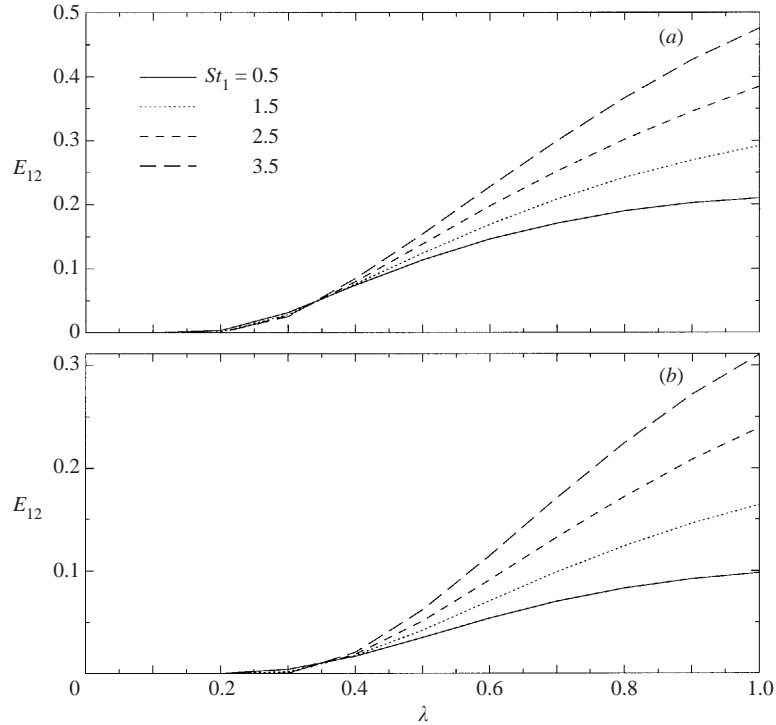


FIGURE 12. Collision efficiency as function of λ for (a) $Q_{12} = 10^3$, (b) $Q_{12} = 10^4$ and for various values of the Stokes number in simple shear flow.

5.2. Pure straining motion

As in the preceding subsection, we begin by comparing our results in the case of a low Stokes number ($St_1 = 10^{-3}$) with those of Wang *et al.* (1994) for inertialess drops. The collision efficiency is first plotted versus the ratio of radii for various values of the viscosity ratio in figure 15. There appears to be no threshold for this type of flow, unlike the pure shear flow. The agreement between our results and those of Wang *et al.* (1994) is good for small values of the viscosity ratio. However, like in the shear flow and probably for the same reason, there is a discrepancy which increases with the viscosity ratio, that is when lubrication effects for close drops become more important. The effect of van der Waals forces is displayed in figure 16, where values of E_{12} are given for $Q_{12} = 1$ and 10, the upper value being chosen for the same reason as in the preceding subsection. As in the case of a simple shear flow, there is a good agreement with the results of Wang *et al.* (1994). Here again, $E_{12} \sim Q_{12}^{-1/n}$, where from regression analysis $n = 3.63, 4.34, 4.66$ for $\lambda = 0.2, 0.5, 1.0$, respectively. There is no possible comparison with Chesters' (1991) results which are limited to the pure shear flow.

Until now, values of E_{12} were found to be smaller than unity. However in a pure straining motion, the collision efficiency can be larger than unity, as remarked at the end of §4. Indeed, the values that we obtain are much larger than unity, as shown in figure 17 for $Q_{12} = 10^3$ and 10^4 . It is observed that for a constant λ , the collision efficiency strongly depends on drop inertia. In particular, for λ close to unity, there is a sharp increase of E_{12} when St_1 varies from 0.5 to 1.5. For large values of St_1 , E_{12} reaches an asymptotic value. For example, when $\lambda = 1$, the value reached at $St_1 = 10^3$

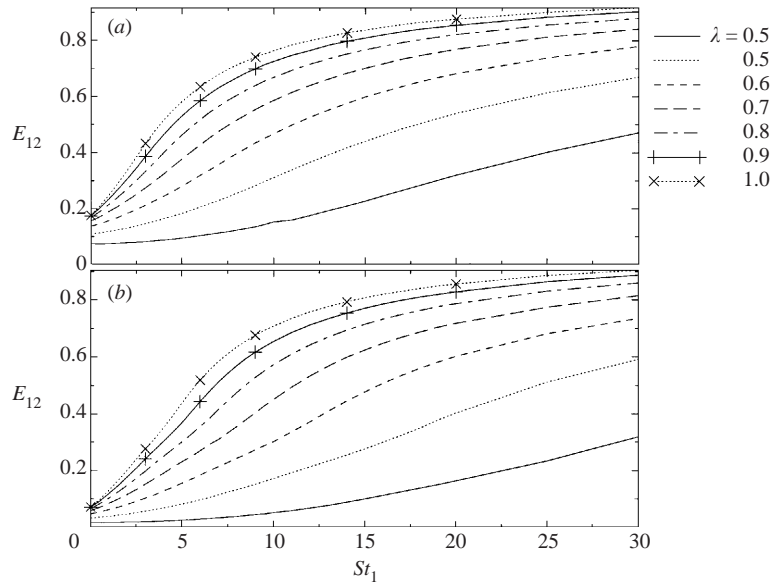


FIGURE 13. Collision efficiency as function of St_1 for (a) $Q_{12} = 10^3$, (b) $Q_{12} = 10^4$ and for various values of the radii ratio in a simple shear flow.

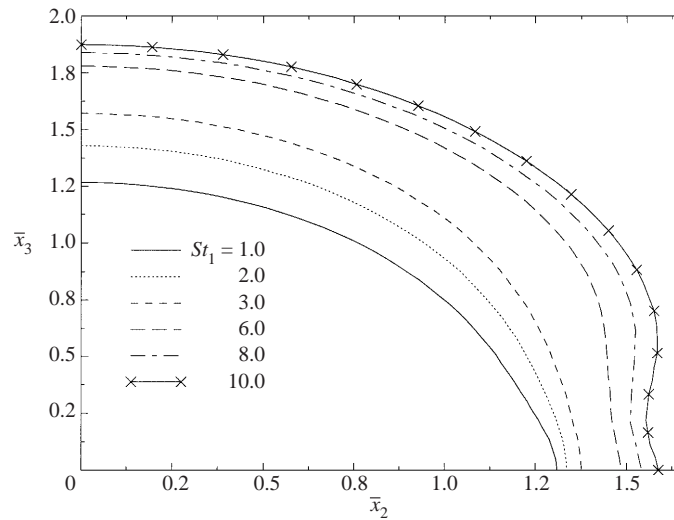


FIGURE 14. Sections of collision for drops of the same size for $Q_{12} = 10^3$ and various values of the Stokes number St_1 .

is $E_{12} \simeq 50$. The only obvious difference between the results for $Q_{12} = 10^3$ and 10^4 is for small Stokes numbers and $\lambda \simeq 1$ since van der Waals forces then become more important than inertial effects.

The sharp increase of E_{12} when St_1 varies from 0.5 to 1.5 is obvious in figure 18 in which E_{12} is represented as function of St_1 for various values of the radii ratio for $Q_{12} = 10^3$ and 10^4 . There is also a rapid increase of the collision efficiency when λ increases from 0.1 to 0.2. This behaviour is connected to the value of the Stokes number of the smaller drop, (4.2).

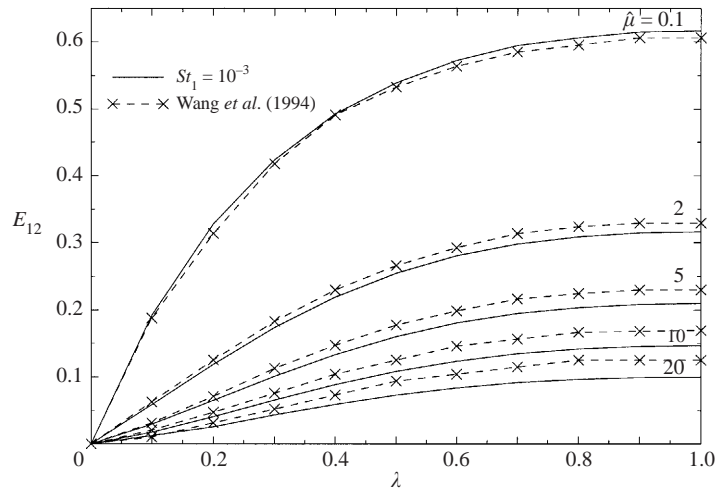


FIGURE 15. Collision efficiency E_{12} of drops in an axisymmetric pure straining motion, as function of λ with $St_1 = 10^{-3}$ and for various values of the viscosity ratio.

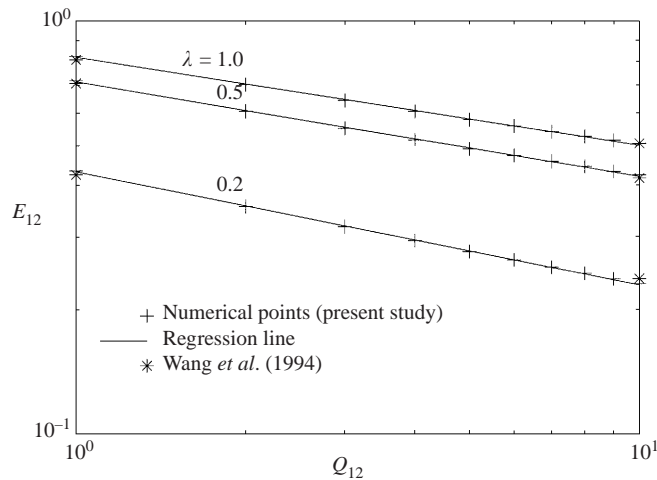


FIGURE 16. Collision efficiency of water drops in air as a function of Q_{12} for small Stokes number, $St_1 = 10^{-3}$, and for $\lambda = 0.2, 0.5,$ and 1 in an axisymmetric pure straining motion.

For $\lambda = 0.1$, the collision is mainly directed by van der Waals forces; the curves for $Q_{12} = 10^3$ and 10^4 (the $\lambda = 0.1$ curves in figure 18a,b) thus are different. As in figure 17, there is also a small difference between the curves for $Q_{12} = 10^3$ and 10^4 for small St_1 , for the reason indicated above.

6. Conclusion

The focus of this article is on the influence of the inertia of drops on their collision efficiency in linear flow fields. Gravity effects are neglected and it is shown that this assumption is compatible with a significant inertia of drops if the shear flow is strong enough. Figure 1 gives an overview of orders of magnitude compatible with the assumptions for the typical case of water drops in air.

A comprehensive set of results is presented for the drag forces on two drops moving in a general linear flow field. This problem is solved by superposition of

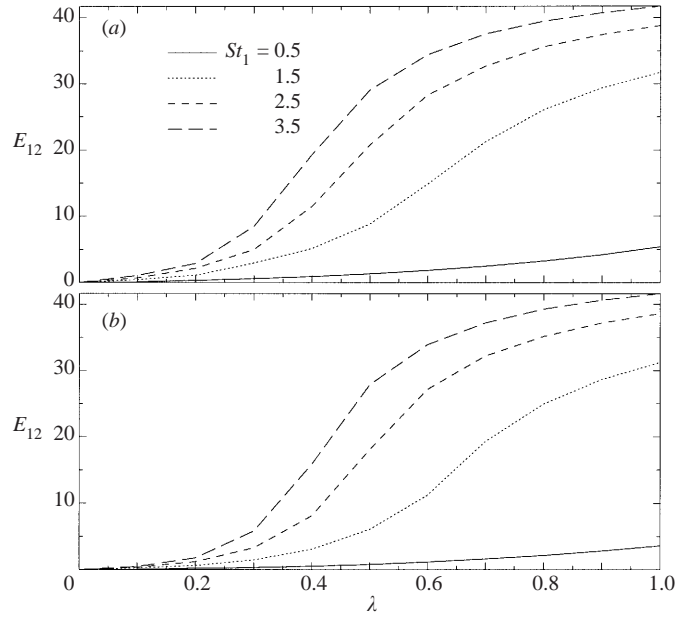


FIGURE 17. Collision efficiency as function of λ for (a) $Q_{12} = 10^3$, (b) 10^4 and for various values of the Stokes number in pure straining motion.

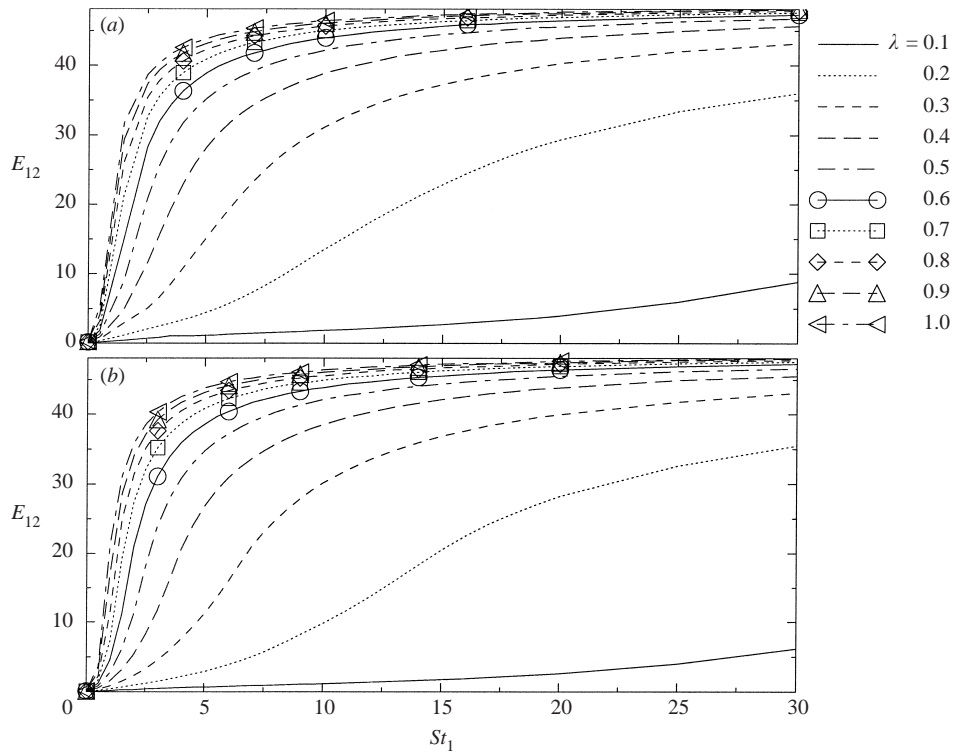


FIGURE 18. Collision efficiency in an axisymmetric pure straining motion as a function of St_1 for (a) $Q_{12} = 10^3$, (b) 10^4 and various values of λ from 0.1 to 1.0.

several elementary linear flow fields (simple shear flows, pure straining motions). Because of drop inertia effects, it is necessary to consider the yet unresolved case of a shear flow parallel to the line of centres. This problem is treated here by two different techniques: the application of the method of bispherical polar coordinates and a superposition of solutions for other flow fields. The results from both approaches are found to be identical within the computational error, thus providing a verification of all calculations and computations involved in these various problems. Finally, a tensorial expression is proposed for the general expressions for the drag forces.

These results for the hydrodynamic forces together with classical expressions for the van der Waals forces then are used to calculate the relative trajectories of two close drops and sections of collision. The calculation is performed for typical linear flow fields, namely a simple shear flow and an axisymmetric pure straining motion. For both flow fields, results obtained for drops with a low Stokes number are in good agreement with those of Wang *et al.* (1994). There is only a small discrepancy for low van der Waals forces (i.e. for large Q_{12}), for nearly equal drops. For non-negligible drop inertia, results show that, as expected, the collision efficiency increases with the Stokes numbers. A surprising result for a shear flow (§5.1) is the presence of a threshold of the collision efficiency E_{12} for a given ratio of radii λ , regardless of the Stokes number St_1 of the larger drop. For $Q_{12} = 10^3$, this threshold is at $\lambda = 0.2$ and for $Q_{12} = 10^4$, it is at $\lambda = 0.3$. The concurrent effects of drop inertia and van der Waals forces appear in the shape of the section of collision: for increasing Stokes number, it becomes anisotropic due to the different relative effects of van der Waals and inertial forces in two perpendicular planes. By comparison, the results for the collision efficiency in an axisymmetric pure straining motion (§5.2) are more regular. This flow field induces strong inertial effects so that the collision efficiency may be much larger than unity. Effects of van der Waals forces become significant only when one of the drops has a very low Stokes number. Since the flow field is axisymmetric, van der Waals forces and inertia effects combine in a simple way.

In conclusion, these results have shown the strong influence of drop inertia. Earlier works omitting this effect while taking into account hydrodynamic interactions underestimate the collision efficiency and this discrepancy may be quite large for a pure straining motion. More elementary approaches ignoring hydrodynamic interactions and inertia effects overestimate (for a pure shear flow) or underestimate (for a pure straining motion) the rate of collision.

Extensions of this work would include a correct account of the close encounter between drops, including gas rarefaction effects (like was done by Davis 1984 for settling particles) and the local deformation of drops. As shown in §2, a description of drop collisions in clouds leading to the formation of rain should also involve coupled effects of sedimentation and linear shear flows. Applications to other fluids could also be considered, provided that the conditions of §2 are satisfied, that is the density ratio $\hat{\rho}$ and the viscosity ratio $\hat{\mu}$ are large compared with unity. Note that $\hat{\mu}$ need not be very large because of the $\hat{\mu}^2$ coefficient in (2.2).

We would like to acknowledge the comments of referees.

Appendix A. The torque on a drop always vanishes

Consider a drop with radius a and surface S . The torque on the drop due to a flow field with stress tensor σ^c is

$$C = \int_S an \times (\sigma^c \cdot n) dS, \quad (\text{A } 1)$$

where \mathbf{n} is the unit vector normal to S . The normal stress gives a zero contribution. The tangential stress is continuous across the interface S . Thus we may replace σ^c by σ^d in (A 1) and obtain the torque on the volume of fluid V inside the drop. This torque vanishes since there is no external applied torque to the fluid and inertia of the fluid motion is negligible.

The consistency with the Stokes equations may be verified in a classical way. Rewriting (A 1) in index notation with Einstein's summation convention and the Levi-Civita alternating tensor:

$$C_i = a \int_S \epsilon_{ijk} n_j \sigma_{kl} n_l dS. \quad (\text{A } 2)$$

Applying the divergence theorem and expanding:

$$C_i = \int_V \frac{\partial}{\partial x_l} \epsilon_{ijk} x_j \sigma_{kl} dV = \int_V \left(\epsilon_{ilk} \sigma_{kl} + \epsilon_{ijk} x_j \frac{\partial}{\partial x_l} \sigma_{kl} \right) dV. \quad (\text{A } 3)$$

The first term vanishes since the stress tensor is symmetric and the second term vanishes from the fluid momentum equation.

Appendix B. Drag forces due to a shear flow along the line of centres

The main formulae are presented here. Details of the derivation may be found in Pigeonneau (1998). Following O'Neill & Majumdar (1998), consider a system of cylindrical coordinates (ρ, θ, z) and the associated bispherical polar coordinates system (ζ, η, θ) defined from

$$z = \frac{c \sinh \zeta}{\cosh \zeta - \cos \eta}, \quad \rho = \frac{c \sin \eta}{\cosh \zeta - \cos \eta}, \quad (\text{B } 1)$$

where c is a geometrical constant. The surface of each drop corresponds to a constant value of ζ (say ζ_1, ζ_2 , respectively). These constants can be fixed by the distance between the centres of the drops and their radii:

$$\cosh \zeta_1 = \frac{s(1+\lambda)}{4} + \frac{(1-\lambda)}{s}, \quad \sinh \zeta_2 = -\frac{\sinh \zeta_1}{\lambda}, \quad c = a_1 \sinh \zeta_1. \quad (\text{B } 2)$$

The determination of the forces is based on the expression for the external flow field, outside the drops. Flows outside and inside the drops are coupled. They are calculated by resolving the Stokes equations.

The external flow field is decomposed as the sum of the unperturbed field and a perturbed field. When written in cylindrical coordinates, the unperturbed field becomes

$$U_\rho^\infty = 0, \quad U_\theta^\infty = 0, \quad U_z^\infty = \gamma_{zx} \rho \cos \theta. \quad (\text{B } 3)$$

The general solutions for the velocity and pressure of the external perturbed field and of those inside of the drops are

$$u_\rho = \left(\frac{\rho}{c} Q + W^1 + W^{-1} \right) \cos \theta, \quad u_\theta = (W^1 - W^{-1}) \sin \theta, \quad u_z = \left(\frac{z}{c} Q + 2W^0 \right) \cos \theta, \quad (\text{B } 4a-c)$$

$$p = \frac{2\mu_c}{c} Q \cos \theta. \quad (\text{B } 5)$$

The functions Q , W^1 , W^{-1} and W^0 are solutions of the partial differential equations

$$L_1^2 Q = 0, \quad L_{1+i}^2 W^i = 0, \quad i = -1, 0, 1, \quad (\text{B } 6a, b)$$

where L_m^2 is an operator defined as

$$L_m^2 = \frac{\partial^2}{\partial \rho^2} + \frac{\partial}{\rho \partial \rho} - \frac{m^2}{\rho^2} + \frac{\partial^2}{\partial z^2}. \quad (\text{B } 7)$$

The results for Q , W^1 , W^{-1} and W^0 are

$$Q = \sqrt{\cosh \zeta - \cos \eta} \sum_{n=1}^{\infty} q_n(\zeta) P_n^1(\cos \eta), \quad (\text{B } 8a)$$

$$W^0 = \sqrt{\cosh \zeta - \cos \eta} \sum_{n=1}^{\infty} w_n^0(\zeta) P_n^1(\cos \eta), \quad (\text{B } 8b)$$

$$W^1 = \sqrt{\cosh \zeta - \cos \eta} \sum_{n=2}^{\infty} w_n^1(\zeta) P_n^2(\cos \eta), \quad (\text{B } 8c)$$

$$W^{-1} = \sqrt{\cosh \zeta - \cos \eta} \sum_{n=0}^{\infty} w_n^{-1}(\zeta) P_n(\cos \eta), \quad (\text{B } 8d)$$

where

$$q_n(\zeta) = C_n e^{-(n+1/2)\zeta} + D_n e^{(n+1/2)\zeta}, \quad (\text{B } 9a)$$

$$w_n^i(\zeta) = A_n^i e^{-(n+1/2)\zeta} + B_n^i e^{(n+1/2)\zeta}, \quad (\text{B } 9b)$$

for $i = 0, 1, -1$. $P_n^m(x)$ is the Legendre function given by (Gradshteyn & Ryzhik 1965, p. 1008).

$$P_n^m(x) = (-1)^m (1-x^2)^{m/2} \frac{d^m P_n(x)}{dx^m}, \quad (\text{B } 10)$$

where $P_n(x)$ is the Legendre polynomial.

Let the superscripts (e) denote the external flow and (1), (2) the flows inside drops 1, 2, respectively. The coefficients A_n, B_n in (B 9b) and C_n, D_n in (B 9a) are determined from the equation of continuity and from the boundary conditions across the drop surfaces. The boundary conditions give

$$\text{for drop 1 : } D_n^{(1)} = B_n^{(1)i} = 0, \forall n \quad \text{and } i = -1, 0, 1, \quad (\text{B } 11a)$$

$$\text{for drop 2 : } C_n^{(2)} = A_n^{(2)i} = 0, \forall n \quad \text{and } i = -1, 0, 1. \quad (\text{B } 11b)$$

The external unperturbed flow can be rewritten with a similar formulation in terms of the function: $W^{\infty 0} = \gamma_{zx} \rho / 2$, in which ρ can be expanded in term of the Legendre function with the identity

$$\rho = -c \sqrt{\cosh \zeta - \cos \eta} 2\sqrt{2} \sum_{n=1}^{\infty} e^{-(n+1/2)|\zeta|} P_n^1(\cos \eta). \quad (\text{B } 12)$$

Thus, the following function is introduced:

$$w_n^{\infty 0}(\zeta) = -c \sqrt{2} \gamma_{zx} e^{-(n+1/2)|\zeta|}. \quad (\text{B } 13)$$

Compared with Zinchenko (1980), there will be some differences in the formulation because of our definition of the Legendre function.

Formulae are made simpler by introducing the auxiliary functions

$$\alpha_n = 5q_n - 2w_n^{-1} + 2(n-1)(n+2)w_n^1, \quad (\text{B } 14a)$$

$$\beta_{n-1} = -(n-1)q_{n-1} + w_{n-1}^{-1} - (n-2)(n-1)w_{n-1}^1, \quad (\text{B } 14b)$$

$$\gamma_{n+1} = (n+2)q_{n+1} + w_{n+1}^{-1} - (n+2)(n+3)w_{n+1}^1, \quad (\text{B } 14c)$$

which, on using (B 9a), (B 9b), can be written in the form

$$\alpha_n(\zeta) = I_n e^{-(n+1/2)\zeta} + J_n e^{(n+1/2)\zeta}, \quad (\text{B } 15a)$$

$$\beta_n(\zeta) = K_n e^{-(n+1/2)\zeta} + K_n e^{(n+1/2)\zeta}, \quad (\text{B } 15b)$$

$$\gamma_n(\zeta) = M_n e^{-(n+1/2)\zeta} + N_n e^{(n+1/2)\zeta}. \quad (\text{B } 15c)$$

This defines the constants $I_n \cdots N_n$ in terms of the $A_n \cdots D_n$.

The equation of continuity for the external flow gives the same relationships as equation 1.8 of Zinchenko (1980):

$$I_n^{(e)} + K_{n-1}^{(e)} + M_{n+1}^{(e)} - 2(2n+1)A_n^{(e)0} + 2(n-1)A_{n-1}^{(e)0} + 2(n+2)A_{n+1}^{(e)0} = 0, \quad (\text{B } 16a)$$

$$J_n^{(e)} + L_{n-1}^{(e)} + N_{n+1}^{(e)} + 2(2n+1)B_n^{(e)0} - 2(n-1)B_{n-1}^{(e)0} - 2(n+2)B_{n+1}^{(e)0} = 0. \quad (\text{B } 16b)$$

The boundary condition of continuity of the tangential fluid velocity across the interface of drop α ($\alpha = 1, 2$) gives three equations:

$$q_n^{(\alpha)} - q_n^{(e)} = \frac{2}{\sinh \zeta_\alpha} \left[\frac{n-1}{2n-1} (Z_{n-1}^{(\alpha)} - w_{n-1}^{\infty 0}) + \frac{n+2}{2n+3} (Z_{n+1}^{(\alpha)} - w_{n+1}^{\infty 0}) - \cosh \zeta_\alpha (Z_n^{(\alpha)} - w_n^{\infty 0}) \right], \quad (\text{B } 17)$$

$$w_n^{(\alpha)-1} - w_n^{(e)-1} = \frac{1}{\sinh \zeta_\alpha} \left[\frac{n(n-1)}{2n-1} (Z_{n-1}^{(\alpha)} - w_{n-1}^{\infty 0}) - \frac{(n+1)(n+2)}{2n+3} (Z_{n+1}^{(\alpha)} - w_{n+1}^{\infty 0}) \right], \quad (\text{B } 18)$$

$$w_n^{(\alpha)1} - w_n^{(e)1} = \frac{-1}{\sinh \zeta_\alpha} \left[\frac{Z_{n-1}^{(\alpha)} - w_{n-1}^{\infty 0}}{2n-1} - \frac{Z_{n+1}^{(\alpha)} - w_{n+1}^{\infty 0}}{2n+3} \right], \quad (\text{B } 19)$$

where

$$Z_n^{(\alpha)} = w_n^{(\alpha)0} - w_n^{(e)0}. \quad (\text{B } 20)$$

Compared with Zinchenko (1980), here there are new terms in $w_n^{\infty 0}$ due to the shear flow with shear rate γ_{zx} , (B 13).

The equations of continuity for the inside flows, when combined with (B 17)–(B 19), give for drop 1

$$I_n^{(e)} + 2(2n+1)A_n^{(e)0} + e^{2\zeta_2} [K_{n-1}^{(e)} - 2(n-1)A_{n-1}^{(e)0}] + e^{-2\zeta_2} [M_{n+1}^{(e)} - 2(n-1)A_{n+1}^{(e)0}] + e^{(n+1/2)\zeta_2} X_n^{(2)} = 0, \quad (\text{B } 21)$$

and for drop 2

$$J_n^{(e)} - 2(2n+1)A_n^{(e)0} + e^{-2\zeta_1} [L_{n-1}^{(e)} + 2(n-1)B_{n-1}^{(e)0}] + e^{2\zeta_1} [N_{n+1}^{(e)} + 2(n-1)B_{n+1}^{(e)0}] + e^{-(n+1/2)\zeta_1} X_n^{(1)} = 0, \quad (\text{B } 22)$$

where

$$X_n^{(\alpha)} = \frac{4}{\sinh \zeta_\alpha} \left[\frac{n-1}{2n-1} (Z_{n-1}^{(\alpha)} - w_{n-1}^{\infty 0}) + \frac{n+2}{2n+3} (Z_{n+1}^{(\alpha)} - w_{n+1}^{\infty 0}) + \left(\frac{|\sinh \zeta_\alpha|}{2n+1} - \cosh \zeta_\alpha \right) (Z_n^{(\alpha)} - w_n^{\infty 0}) \right]. \quad (\text{B } 23)$$

The condition of zero normal velocity across the interface of drop α at rest gives, using the β_n , γ_n , defined in (B 14b), (B 14c), respectively

$$\frac{\gamma_{n+1}^{(e)}}{2n+3} - \frac{\beta_{n-1}^{(e)}}{2n-1} + \frac{2 \cosh \zeta_\alpha}{\sinh \zeta_\alpha} \left[\frac{(n-1)(w_{n-1}^{(t)0})}{2n-1} + \frac{(n+2)(w_{n+1}^{(t)0})}{2n+3} \right] - \frac{2w_n^{(t)0}}{\sinh \zeta_\alpha} = 0, \quad (\text{B } 24)$$

where

$$w_n^{(t)0} = w_n^{(e)0} + w_n^{\infty 0}. \quad (\text{B } 25)$$

The tangential stress should be continuous across the interface of drop α . Results again differ from Zinchenko (1980) in the new terms in $w_n^{\infty 0}$. The component located in the meridian plane gives after a few manipulations

$$\begin{aligned} & \frac{3(\hat{\mu}-1)}{\hat{\mu}+1} \left[\sinh \zeta_\alpha q_n^{(e)} + 2 \left(\cosh \zeta_\alpha w_n^{(t)0} - \frac{n-1}{2n-1} w_{n-1}^{(t)0} - \frac{n+2}{2n+3} w_{n+1}^{(t)0} \right) \right] \\ & + \cosh \zeta_\alpha \left[\frac{n+2}{2n+3} (\gamma_{n+2}^{(e)\pm} - \beta_n^{(e)\pm}) + \frac{n-1}{2n-1} (\gamma_n^{(e)\pm} - \beta_{n-2}^{(e)\pm}) - (2n+1) q_n^{(e)\pm} \right] \\ & + 2 \sinh \zeta_\alpha \left[\frac{(n-1)(n-2)}{2n-1} w_{n-2}^{t\pm} + \frac{(n+2)(n+3)}{2n+3} w_{n+2}^{t\pm} - \frac{2n(n+1)(2n+1)}{(2n-1)(2n+3)} w_n^{t\pm} \right] \\ & + \beta_{n-1}^{(e)\pm} - \gamma_{n+1}^{(e)\pm} + (n-1) q_{n-1}^{(e)\pm} + (n+2) q_{n+1}^{(e)\pm} \\ & + \frac{4\hat{\mu}}{(\hat{\mu}+1)|\sinh \zeta_\alpha|} \left\{ \frac{(n-2)(n-1)}{(2n-1)(2n-3)} (Z_{n-2}^{(z)} - w_{n-2}^{\infty 0}) \right. \\ & - \frac{2(n-1)^2}{(2n-1)^2} \cosh \zeta_\alpha (Z_{n-1}^{(z)} - w_{n-1}^{\infty 0}) + \frac{2}{2n+1} \left[\frac{2n(n+1)}{(2n+3)(2n-1)} - 1 \right] (Z_n^{(z)} - w_n^{\infty 0}) \\ & \left. + \frac{2(n+2)^2}{(2n+3)^2} \cosh \zeta_\alpha (Z_{n+1}^{(z)} - w_{n+1}^{\infty 0}) - \frac{(n+2)(n+3)}{(2n+3)(2n+5)} (Z_{n+2}^{(z)} - w_{n+2}^{\infty 0}) \right\} = 0, \quad (\text{B } 26) \end{aligned}$$

where the function f_n^\pm is defined by

$$f_n^\pm = \frac{(df_n/d\zeta) \pm \hat{\mu}(n + \frac{1}{2})f_n}{(n + \frac{1}{2})(\hat{\mu} + 1)}. \quad (\text{B } 27)$$

The component in direction θ , when combined with the continuity equations outside and inside the drops, gives

$$q_n^{(e)\pm} = \frac{2(1-\hat{\mu})}{\hat{\mu}+1} \left\{ \frac{\sinh \zeta_\alpha}{2n+3} \gamma_{n+1}^{(e)} + \frac{2(n+2) \cosh \zeta_\alpha}{2n+3} w_{n+1}^{(t)0} - w_n^{(t)0} \right\} \mp \frac{\hat{\mu}}{2(\hat{\mu}+1)} X_n^{(z)}. \quad (\text{B } 28)$$

The forces on drops 1 and 2 are given by

$$F_{1x} = 8\sqrt{2}\pi\mu_c c \sum_{n=1}^{\infty} n(n+1)D_n^{(e)0}, \quad F_{2x} = 8\sqrt{2}\pi\mu_c c \sum_{n=1}^{\infty} n(n+1)C_n^{(e)0}. \quad (\text{B } 29a, b)$$

The numerical method to find F_{1x} and F_{2x} is identical to that of Zinchenko (1980). It can be verified that the sums are proportional to γ_{zx} , as expected. The coefficients

D_1^{zx} , D_2^{zx} defined in (3.10a), (3.10b), then are given by

$$D_1^{zx} = -\frac{4}{3}\sqrt{2}\sinh^2\zeta_1 \frac{\sum_{n=1}^{\infty} n(n+1)D_n^{(e)0}}{c\gamma_{zx}}, \quad (\text{B } 30a)$$

$$D_2^{zx} = \frac{4}{3}\sqrt{2}\sinh\zeta_1 \sinh\zeta_2 \frac{\sum_{n=1}^{\infty} n(n+1)C_n^{(e)0}}{c\gamma_{zx}}. \quad (\text{B } 30b)$$

REFERENCES

- BATCHELOR, G. K. & GREEN, J. T. 1972 The hydrodynamic interaction of two small freely-moving spheres in a linear flow field. *J. Fluid Mech.* **56**, 375–400.
- BREHERTON, F. P. 1962 The motion of rigid particles in a shear flow at low Reynolds number. *J. Fluid Mech.* **14**, 284–304.
- CHESTERS, A. K. 1991 The modelling of coalescence processes in fluid-liquid dispersions: A review of current understanding. *Trans. Inst. Chem. Engrs.* **69**, 259–270.
- DAVIS, R. H. 1984 The rate of coagulation of a dilute polydisperse system of sedimenting spheres. *J. Fluid Mech.* **145**, 179–199.
- DAVIS, R. H., SCHONBERG, J. A. & RALLISON, J. M. 1989 The lubrication force between two viscous drops. *Phys. Fluids A* **1**, 77–81.
- FUCHS, N. A. 1964 *The Mechanics of Aerosols*. Pergamon.
- GRADSHTEYN, I. S. & RYZHIK, I. M. 1965 *Table of Integrals, Series and Products*. Academic.
- HADAMARD, J. 1911 Mouvement permanent lent d'une sphère liquide et visqueuse dans un liquide visqueux. *C. R. Acad. Sci. Paris* **152**, 1735–1738.
- HABER, S., HETSRONI, G. & SOLAN, A. 1973 On the low Reynolds number motion of two droplets. *Intl J. Multiphase Flow* **1**, 57–71.
- HAMAKER, H. C. 1937 The London-van der Waals attraction between spherical particles. *Physica* **4**, 1058–1072.
- HETSRONI, G. & HABER, S. 1978 Low Reynolds number motion of two drops submerged in an unbounded arbitrary velocity field. *Intl J. Multiphase Flow* **4**, 1–17.
- HOCKING, L. M. & JONAS, P. R. 1970 The collision efficiency of small drops. *Q. J. R. Met. Soc.* **96**, 722–729.
- JEFFREY, D. J. 1992 The calculation of the low Reynolds number resistance functions for two unequal spheres. *Phys. Fluids A* **4**, 16–29.
- JEFFREY, D. J. & ONISHI, Y. 1984 Calculation of the resistance and mobility functions for two unequal rigid spheres in low-Reynolds-number flow. *J. Fluid Mech.* **139**, 261–290.
- JEFFERY, G. B. 1912 On a form of the solution of Laplace's equation suitable for problems relating to two spheres. *Proc. R. Soc. Lond.* **87**, 109–120.
- JONAS, P. R. 1972 The collision efficiency of small drops. *Q. J. R. Met. Soc.* **98**, 681–683.
- JONAS, P. R. 1996 Turbulence and cloud microphysics. *Atmos. Res.* **40**, 283–306.
- KAPS, P. & RENTROP, P. 1979 Generalized Runge-Kutta methods of order four with stepsize control for stiff ordinary differential equations. *Numer. Maths* **33**, 55–68.
- KIM, S. & KARRILA, S. P. 1991 *Microhydrodynamics: Principles and Selected Applications*. Butterworth-Heinemann.
- LIN, C. J. 1968 Statistical mechanical theory of shock waves and suspensions. PhD thesis, University of Washington.
- O'NEILL, M. E. & MAJUMDAR, S. R. 1970 Asymmetrical slow viscous fluid motions caused by the translation or rotation of two spheres. Part I: The determination of exact solutions for any values of the ratio of radii and separation parameters. *Z. Angew. Math. Phys.* **21**, 164–179.
- PIGEONNEAU, F. 1998 Modélisation et calcul numérique des collisions de gouttes en écoulements laminaires et turbulents. PhD thesis, Université Pierre et Marie Curie, Paris VI.

- PRESS, W. H., TEUKOLSKY, S. A., VETTERLING, W. T. & FLANNERY, B. P. 1992 *Numerical Recipes in Fortran 77*. Cambridge University Press.
- RYBCZYNSKI, W. 1911 Über die fortschreitende Bewegung einer flüssigen Kugel in einem zähen Medium. *Bull. Inst. Acad. Sci. Cracovie*, A 40–46.
- SMOLUCHOWSKI, M. V. 1917 Versuch einer mathematischen Theorie der Koagulationskinetik kolloider Lösungen. *Z. Phys. Chem.* **92**, 129–168.
- STIMSON, M. & JEFFERY, G. B. 1926 The motion of two spheres in a viscous fluid. *Proc. R. Soc. Lond. A* **111**, 110–116.
- WANG, H. W., ZINCHENKO, A. Z. & DAVIS, R. H. 1994 The collision rate of small drops in linear flow fields. *J. Fluid Mech.* **265**, 161–188.
- ZINCHENKO, A. Z. 1980 The slow asymmetric motion of two drops in a viscous medium. *Prikl. Matem. Mekhan.* **44**, 49–59.
- ZINCHENKO, A. Z. 1982 Calculation of the effectiveness of gravitational coagulation of drops with allowance for internal circulation. *Prikl. Matem. Mekhan.* **46**, 72–82.
- ZEICHNER, G. R. & SCHOWALTER, W. R. 1977 Use of trajectory analysis to study stability of colloidal dispersions in flow fields. *AIChE J.* **23**, 243–254.